An Investigation of Compensation Networks for Three-coil Wireless Power Transfer

WANG H.S.[1] CHENG K.W.E.[2] HU J.F.[3]

[1,2] Power Electronics Research Centre, Department of Electrical Engineering, The Hong Kong Polytechnic University, Hong Kong
[3] School of Engineering, Information Technology and Physical Sciences, Federation University, Australia
[1]E-mail: herschel.wang@connect.polyu.hk

Abstract –Wireless power transfer (WPT) can power loads over large air gaps with relatively high efficiency, offering an innovative and convenient charging way. Especially, three-coil WPT shows the superiority, namely, the extended transmission distance with high efficiency. However, compensation networks in three-coil WPT still necessitate investigation. In this paper, three compensation topologies including S-S-S, S-S-P and N-S-S are investigated. Some important characteristics including load-independent constant voltage (CV), load-independent constant current (CC) and zero voltage switching (ZVS) are concluded and compared among different topologies. Detailed design procedures of compensation networks based on three-coil couplers are demonstrated. The fundamental analysis, coil design, compensation topologies and experimental verification are all presented and discussed in this paper.

Keywords – Wireless power transfer, compensation topology, three-coil, constant output

I. Introduction

Wireless power transfer (WPT) is an outstanding technology that can transfer energy via time-varying magnetic fields [1]. Electrical apparatus equipped with WPT are able to beat conventionally contact-based methods because of no physical contact between from the source to the load. In other words, WPT can offer a versatile energization manner that gets rid of troubles from messy cables and the environmental constraint, which is gradually popular in electric vehicles [2, 3], heating systems [4, 5], light emitting diode (LED) driver [6, 7], consumer electronics [8] and mobile device [9, 10]. Considerable research efforts have been devoted to two-coil WPT due to its simplicity, which usually consists of one transmitter (Tx) and one receiver (Rx) [11-13]. In traditional two-coil WPT systems, there are basic four topologies, i.e., series–series (SS) [14], series–parallel (SP) [15], parallel–series (PS) [16], and parallel–parallel (PP) [17] as shown in Fig. 1.

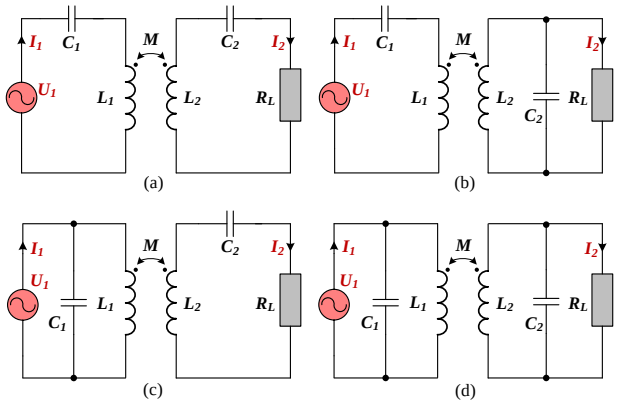

Fig. 1: Four basic compensation networks in two-coil WPT
(a) SS. (b) SP. (c) PS. (d) PP.

Recently, three-coil WPT is gaining increasing attention from researchers and engineers [18-21]. A typical three-coil WPT system consists of three coils, i.e., a transmitter (T_X), a relay coil and a receiver coil (R_X). In general, there are four typical types of three-coil WPT systems including type-A, B and C as shown in Fig. 2. The classification is according to the value of the mutual inductance between the Tx and the Rx, i.e., M_2 and the relevant positions of three coils. Detailed classification data is shown in Table. 1.

Table 1: One classification of three-coil WPT

Three-coil WPT with nonnegligible M_2	Three-coil WPT with negligible M_2		
TYPE-A	TYPE-B	TYPE-C	TYPE-D
[22, 23]	[24, 25]	[26, 27]	[7, 18, 19, 21, 28, 29]

Specifically, type A is the scenario with the nonnegligible M_2. By contrast, M_2 can be deliberately designed to be tiny enough to a negligible level from type B to D. Type B is the scenario where the relay coil is placed near the receiver. In type B, the load impedance is able to be reflected to obtain an optimal value, thereby realizing both arbitrary load impedance to the optimal value as well as high power delivery [24]. In terms of type C, the relay coil is placed to be equidistant between the transmitter and the receiver with the same distance to ensure expected mutual inductances [26] or the desired voltage gain [27].

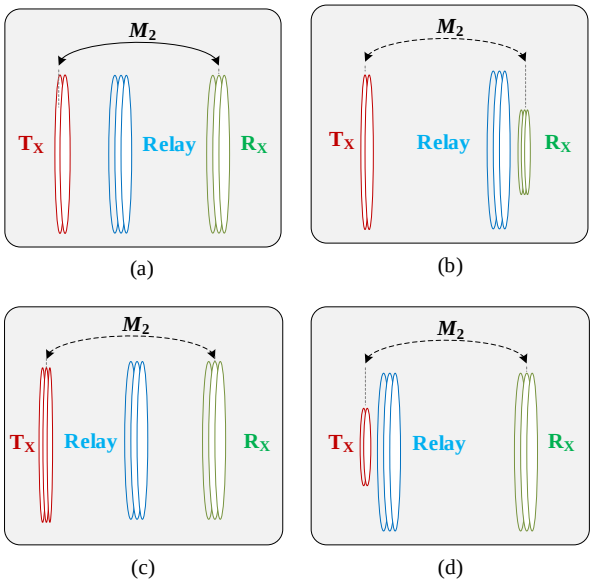

Fig. 2: Four typical types of three-coil WPT
(a) TYPE-A. (b) TYPE-B. (c) TYPE-C. (d) TYPE-D.

II. Coupling Structure Design

In this paper, only type D is considered and adopted owing to its intrinsic superiority, i.e., the extended transmission distance with high efficiency [13, 14]. One normal practice of type D is to shrink the size of transmitter coil with extended transmission distance to achieve an exceedingly small M_2. That means the influence from M_2 can be ignorable. Moreover, the relay coil from the type D saves room since it does not take up much space between the T_X and R_X compared to traditional two-coil structures [13]. Thus, the coupling structure in this paper consists of three coils in total, namely, transmitter, relay and receiver are demonstrated in Fig. 3. The airgap between T_X and relay is D_0 while the airgap between relay and R_X is D_1. Particularly, D represents the transmission distance from T_X to R_X, which is also the sum of D_0 and D_1.

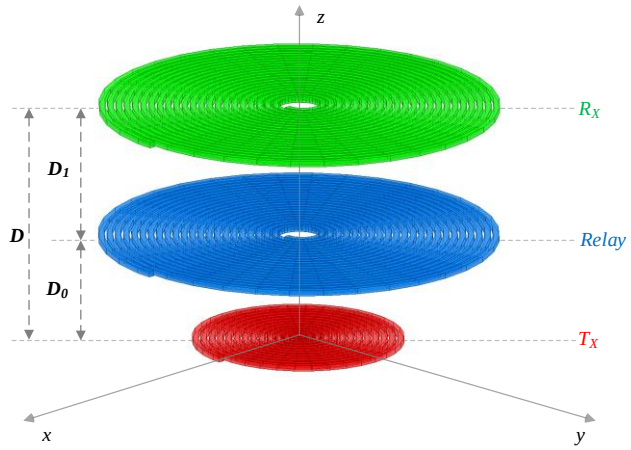

Fig. 3: The scheme of the coupling structure

As illustrated in Fig. 4, the parameters of these three coils are well designed by finite element analysis (FEA). Essential parameters are taken into consideration including inner diameter d_{in}, outer diameter d_{out}, wire diameter d_w, turn spacing S and turns N. Detailed parameter information from the magnetic coupling structure is able to be found in Table 2.

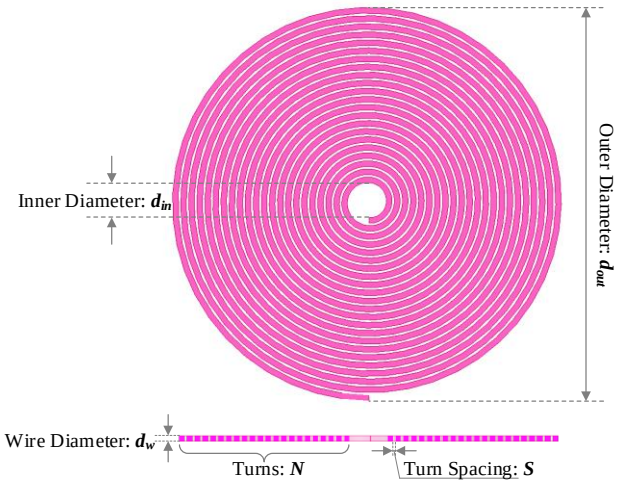

Fig. 4: The diagram of the coil design

Table 2: Detailed parameters of the coil design

Parameter / Coil	d_{out} (mm)	d_{in} (mm)	d_w (mm)	S (mm)	N
T_X	75	10	2.1	0.663	12
Relay	20	20	2.1	0.895	22
R_X	150	150	2.1	0.895	22

III. Circuit Analysis

The circuit scheme of an entire three-coil WPT system is illustrated in Fig. 5. V_{dc} is the input dc voltage from regulated DC power supply. An inverter is adopted from the transmitter side to generate 200kHz AC power into the transmitter with an operating angular frequency ω. Specifically, L_1, L_r, and L_2 are the self-inductances of the T_X, the relay coil and the R_X with corresponding equivalent series resistances R_1, R_r and R_2 respectively [28]. The mutual inductance between the T_X and the relay coil is M_1 while the mutual inductance between the relay coil and the R_X is M_3. It is noteworthy that M_2, the mutual inductance between the T_X and the R_X, is delicately designed to be exceedingly small for simplifying analysis and reducing the cross-coupling effect. The fundamental component of the output voltage from the inverter can be expressed as [28]

$$u_1(t) = \frac{4V_{dc}}{\pi}\sin \omega t \tag{1}$$

The corresponding fundamental phasor can be given as

$$\dot{U}_1 = \frac{2\sqrt{2}}{\pi}V_{dc}\angle 0^\circ \tag{2}$$

A full-bridge rectifier is used after the receiver. R_{eq} denotes the equivalent load from the rectifier, which is gained as [28]

$$R_{eq} = \frac{8}{\pi^2}R_L \tag{3}$$

The output voltage on the load is represented by V_L. And U_O is the RMS value of the input voltage for the rectifier. The relationship between them can be expressed as

$$V_L = \frac{\pi U_O}{2\sqrt{2}} \tag{4}$$

Three compensation parts are also shown with related coils, which includes T_X compensation, relay compensation and R_X compensation. It is necessary to utilize compensation networks for minimizing VA rating and maximizing power transfer capability, achieving load-independent constant-voltage (CV) or current output (CC), improving efficiency and impeding bifurcation phenomenon [30]. Currently, the voltage-source inverter (VSI) is widely used for powering WPT systems, resulting in P compensation cannot be directly connected to the VSI [31]. Furthermore, relay coils tend to be simple and non-configurable, therefore, only S compensation can be connected with such a relay coil like [7], [28], [32]. Accordingly, three compensation types are concluded in Table.2, including S-S-S, S-S-P and N-S-S compensation networks.

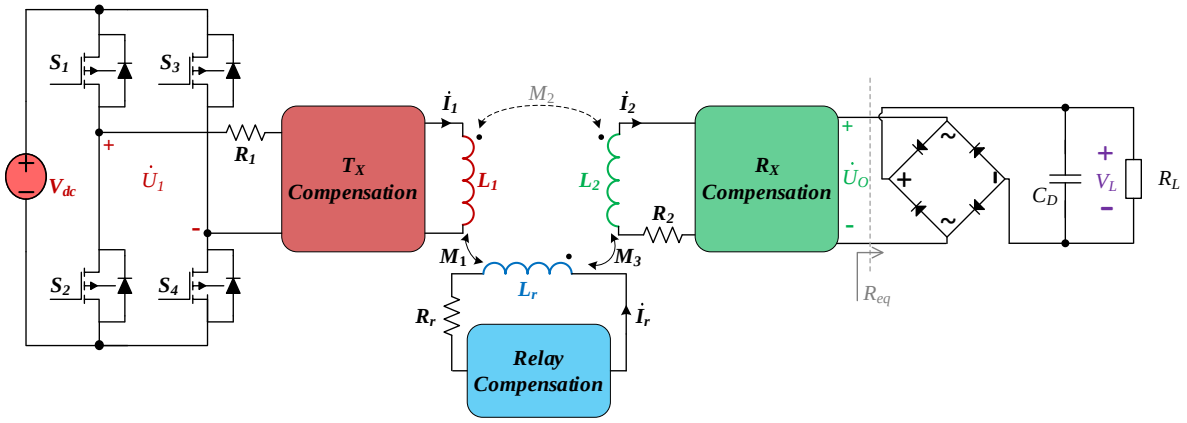

Fig. 5: The entire circuit scheme of the proposed three-coil WPT system

Table 2: Summary of compensation networks

Type	Equivalent Circuit Diagram
S-S-S	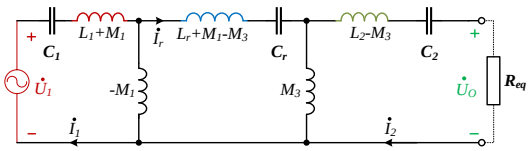
S-S-P	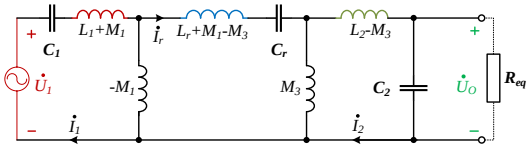
N-S-S	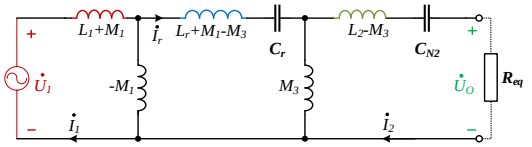

A. S-S-S Type

The S-S-S compensation topology is able to fulfill the load-independent output voltage [7, 28, 32]. For tuning the coils and achieving CV output, the operating angular frequency ω should meet the equation:

$$\omega = \sqrt{\frac{1}{L_1 C_1}} = \sqrt{\frac{1}{L_r C_r}} = \sqrt{\frac{1}{L_2 C_2}} \tag{5}$$

According to [28], the voltage gain from the source to the equivalent load from S-S-S compensation topology can be written as

$$\frac{\dot{U}_1}{\dot{U}_O} = \frac{M_3}{M_1} \tag{6}$$

By designing coupler deliberately, M_1 is equal to M_3 in this paper. Hence, the following relationship equations between the source part and the load side can be simplified and rewritten as

$$\dot{U}_O = \dot{U}_1 \tag{7}$$

$$\dot{I}_O = \frac{\dot{U}_1}{R_{eq}} \tag{8}$$

$$Z_{sss} = \dot{U}_1 / \dot{I}_1 = R_{eq} \tag{9}$$

B. S-S-P Type

For tuning the coils and achieving CC output, the operating angular frequency ω should satisfy the equation (5) too. Then voltage relationship between the source part and the load side can be yielded:

$$\dot{U}_O = \frac{R_{eq}}{j\omega L_2}\dot{U}_1 \tag{10}$$

The output current flowing through R_{eq} can be derived as

$$\dot{I}_O = \frac{\dot{U}_1}{j\omega L_2} \tag{11}$$

The value of this output current is associated with the operating frequency ω, the self-inductance value of the R_X, and output voltage of the inverter. That means it is desirable to gain the objective output current by designing component parameters deliberately. And the input impedance of S-S-P is able to be gained as

$$Z_{ssp} = \dot{U}_1 / \dot{I}_1 = \frac{\omega^2 {L_2}^2 R_{eq}}{{R_{eq}}^2 + \omega^2 {L_2}^2} + j\frac{\omega^3 {L_2}^3}{{R_{eq}}^2 + \omega^2 {L_2}^2} \tag{12}$$

It is noted that there is an imaginary component in Z_{ssp}, thereby making the whole system inductive and improving the VA rating.

C. N-S-S Type

The N from N-S-S represents there is no compensation network from the transmitter part in this topology. Then, the compensation network from the receiver part should take the responsibility for tuning the transmitter part [33]. Therefore, the capacitor in the receiver side C_{N2} can be expressed as

$$C_{N2} = \frac{1}{\omega^2 (L_1 + L_2)} \tag{13}$$

Similarly, the load-independent output voltage can be gained as

$$\dot{U}_O = \dot{U}_1 \tag{14}$$

This voltage is only related to the output voltage from the inverter. Then, the current flowing through R_{eq} can be derived as

$$\dot{I}_O = \frac{1}{R_{eq}}\dot{U}_1 \tag{15}$$

Therefore, the input impedance of N-S-S network can be expressed as

$$Z_{nss} = \dot{U}_1 / \dot{I}_1 = R_{eq} \tag{16}$$

IV. Experimental Validation

An experimental platform has been built up to validate the availability of the theoretical analysis as illustrated in Fig.6. All the coils are made of 250-strand LITZ wire to form inductors, which dramatically reduces the skin effect. The operating frequency from the inverter is set to be 200kHz. One switch and two resistive loads are used to verify transient response when the load change happens. Experimental waveforms are directly gained and analyzed from oscilloscope Tektronix MDO3024. The two output channels from power supply EZ Digital GP-1305DU are connected in series to constantly provide 50V as the DC input voltage to feed the inverter. And the measured parameters of the entire prototype are shown in Table. 3.

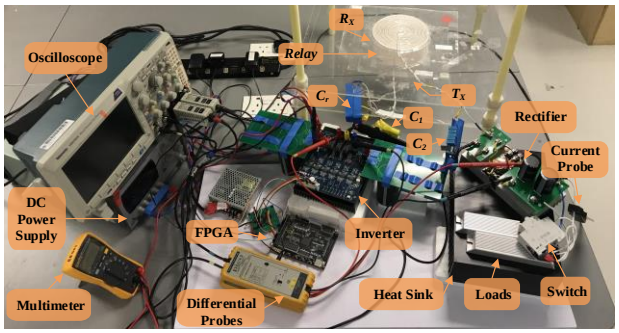

Fig. 6: Experimental Prototype

Table 3: Measured parameters

L_1	L_r	L_2	M_1	M_3
4.63μH	32.62μH	29.51μH	4.65μH	4.65μH
C_1	C_r	C_2	C_{N2}	f
137.05nF	19.32nF	21.10nF	18.47nF	200kHz
R_1	R_r	R_2	D_0	D_1
0.04Ω	0.20Ω	0.17Ω	0.5cm	6.5cm

A. S-S-S Experimental Results

Fig. 7 depicts the essential waveforms from the inverter and the output voltage on the load part. It is noteworthy that the current slightly lags corresponding voltage, which indicates ZVS can be achieved in this topology.

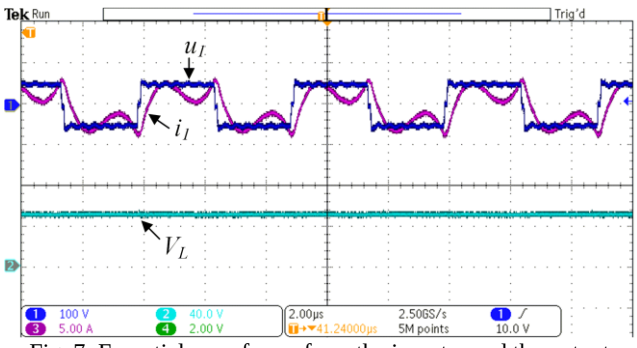

Fig. 7: Essential waveforms from the inverter and the output voltage on the load in S-S-S type

Fig. 8 demonstrates the transient response of S-S-S topology. Even though the output current from the load experiences a sharp rise and down, the output voltage keeps stable around 50V. Indicated by the oscilloscope, the change of voltage is 2.4V. In other words, the voltage fluctuation is 4.8% from 50.4 V to 48V while the load drops by 50%.

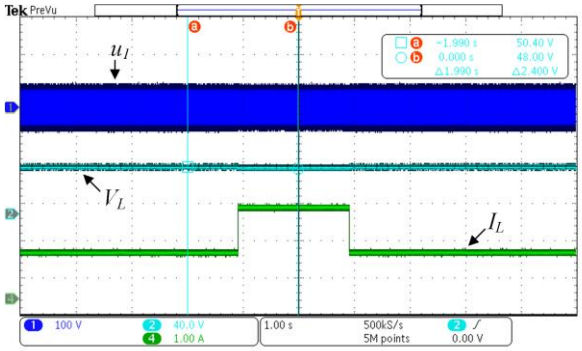

Fig. 8: Transient response when the load is changed from 40Ω to 20Ω and back to 40Ω in S-S-S type

B. S-S-P Experimental Results

Fig. 9 illustrates the essential waveforms from the inverter at the T_X side and the output voltage on the load. Nevertheless, the equivalent impedance is inductive so that i_1 lags u_1 around 90 degrees. Therefore, the reactive power cannot be ignored in this topology.

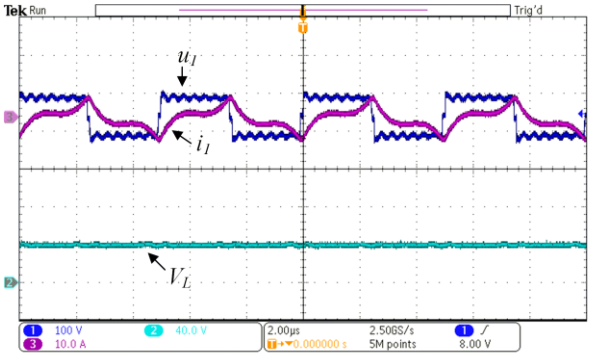

Fig. 9: Essential waveforms from the inverter and the output voltage on the load in S-S-P type

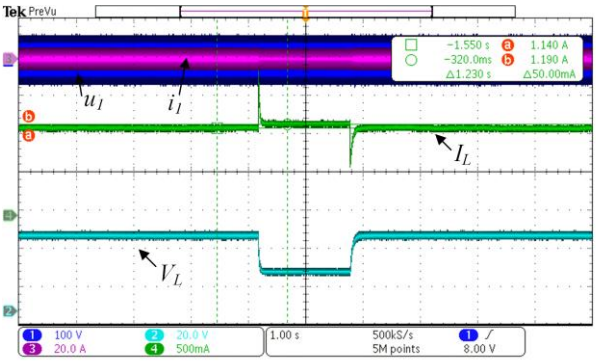

Fig. 10: Transient response when the load changes from 40Ω to 20Ω and back to 40Ω in S-S-P type

Fig. 10 manifests the measured waveforms of u_1, i_1, V_L and I_L when the load is between 40Ω and 20Ω, respectively. The current is changed from 1.19A to 1.14A with overshoots.

The oscillation of the current is 50mA. The output current declines by 4.2% and the load falls by 50%.

C. N-S-S Experimental Results

The steady-mode waveforms of u_1, i_1, V_L and I_L are shown in Fig. 11 at R_L=40Ω, which illustrates that the current i_1 slightly lags u_1. This manifests ZVS can also be achieved in this topology.

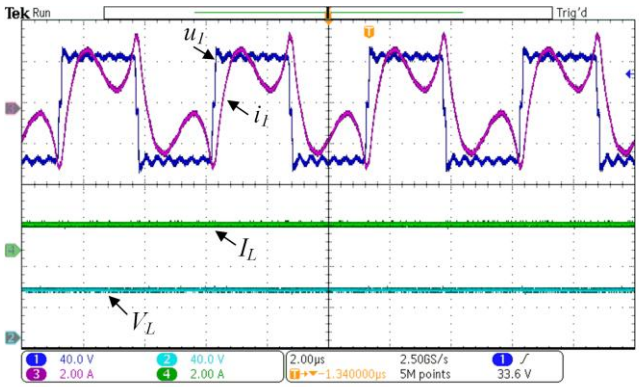

Fig. 11: Essential waveforms from the inverter and the output voltage on the load in N-S-S type

Fig.12 depicts the transient response of N-S-S topology. When the load is 40 Ω, the output voltage is 45.6V. Then the load is reduced to 20Ω, and the output voltage becomes 44.8V. The voltage change is only 0.8V, which can be directly detected from the oscilloscope. The output voltage declines by 1.8% and the load falls by 50%.

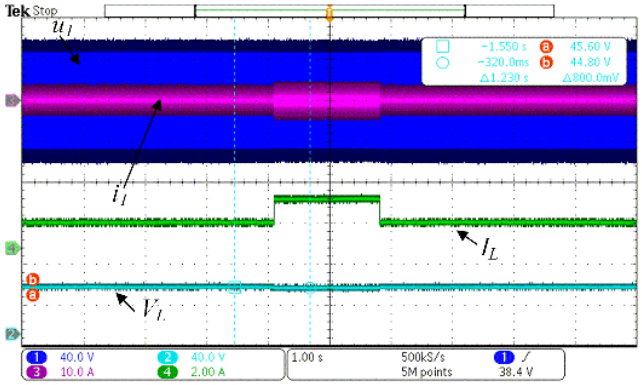

Fig. 12: Transient response when the load changes from 40Ω to 20Ω and back to 40Ω in N-S-S type

V. Conclusion

In this paper, three compensation networks, namely, S-S-S, S-S-P and N-S-S are studied for three-coil WPT systems. Coupling structure design, circuit analysis and experimental verification are all conducted to investigate key characteristics such as load-independent CC or CV outputs and ZVS. All coils are designed by the finite element analysis software carefully. A summary of the compensation network is also demonstrated with equivalent T-model circuits. Key waveforms with related description have been shown and discussed. An experimental prototype is managed to be built up and corresponding experimental results successfully show the agreement with the theoretical analysis. In the future, WPT systems equipped with these compensation networks could be scaled down or up for wirelessly charging consumer electronics or EVs.

References

[1] Y. Li, J. Hu, K. W. Chan, K. W. E. Cheng, and M. Liu, "A Flexible Load-Independent Multi-Output Wireless Power Transfer System Based on Double-T Resonant Circuit Technique," in *2018 IEEE Energy Conversion Congress and Exposition (ECCE)*, 23-27 Sept. 2018 2018, pp. 3593-3596.

[2] K. W. K. Chen and K. W. E. Cheng, "Review of magnetic resonance technology, recent research trends and issues in EV wireless charging," in *The 11th IET International Conference on Advances in Power System Control, Operation and Management (APSCOM 2018)*, 11-15 Nov. 2018 2018, pp. 1-7.

[3] Y. C. Fong and K. W. E. Cheng, "A switched-capacitor step-up inverter for bidirectional wireless charging applications in electric microcar," in *2017 7th International Conference on Power Electronics Systems and Applications - Smart Mobility, Power Transfer & Security (PESA)*, 12-14 Dec. 2017 2017, pp. 1-6.

[4] L. Meng and K. W. E. Cheng, "Wireless power transfer technology for electric iron based on multi-coils induction heating design," *IET Power Electronics,* vol. 12, no. 10, pp. 2566-2577, 2019, doi: 10.1049/iet-pel.2018.6305.

[5] L. C. Meng, K. W. E. Cheng, and W. M. Wang, "Thermal Impacts of Electromagnetic Proximity Effects in Induction Cooking System With Distributed Planar Multicoils," *IEEE Transactions on Magnetics,* vol. 47, no. 10, pp. 3212-3215, 2011.

[6] Y. Li *et al.*, "Analysis, Design, and Experimental Verification of a Mixed High-Order Compensations-Based WPT System with Constant Current Outputs for Driving Multistring LEDs," *IEEE Transactions on Industrial Electronics,* vol. 67, no. 1, pp. 203-213, 2020.

[7] Y. Li, J. Hu, X. Li, H. Wang, and K. W. E. Cheng, "Cost-Effective and Compact Multistring LED Driver Based on a Three-Coil Wireless Power Transfer System," *IEEE Transactions on Power Electronics,* vol. 34, no. 8, pp. 7156-7160, 2019.

[8] X. Li, J. Hu, Y. Li, H. Wang, M. Liu, and P. Deng, "A Decoupled Power and Data-Parallel Transmission Method With Four-Quadrant Misalignment Tolerance for Wireless Power Transfer Systems," *IEEE Transactions on Power Electronics,* vol. 34, no. 12, pp. 11531-11535, 2019.

[9] X. Li, J. Hu, H. Wang, X. Dai, and Y. Sun, "A New Coupling Structure and Position Detection Method for Segmented Control Dynamic Wireless Power Transfer Systems," *IEEE Transactions on Power Electronics,* vol. 35, no. 7, pp. 6741-6745, 2020.

[10] Y. Li *et al.*, "A New Coil Structure and Its Optimization Design With Constant Output Voltage and Constant Output Current for Electric Vehicle Dynamic Wireless Charging," *IEEE Transactions on Industrial Informatics,* vol. 15, no. 9, pp. 5244-5256, 2019.

[11] X. Li, C. Tang, X. Dai, P. Deng, and Y. Su, "An Inductive and Capacitive Combined Parallel Transmission of Power and Data for Wireless Power Transfer Systems," *IEEE Transactions on Power Electronics,* vol. 33, no. 6, pp. 4980-4991, 2018.

[12] X. Dai, X. Li, Y. Li, and A. P. Hu, "Maximum Efficiency Tracking for Wireless Power Transfer Systems With Dynamic Coupling Coefficient Estimation," *IEEE Transactions on Power Electronics,* vol. 33, no. 6, pp. 5005-5015, 2018.

[13] D. Patil, M. K. McDonough, J. M. Miller, B. Fahimi, and P. T. Balsara, "Wireless Power Transfer for Vehicular Applications: Overview and Challenges," *IEEE Transactions on Transportation Electrification,* vol. 4, no. 1, pp. 3-37, 2018.

[14] Z. Zhang, H. Pang, A. Georgiadis, and C. Cecati, "Wireless Power Transfer—An Overview," *IEEE Transactions on Industrial Electronics,* vol. 66, no. 2, pp. 1044-1058, 2019.

[15] B. J. Varghese, A. Kamineni, and R. A. Zane, "Empirical Closed-Form Analysis for Inductance and Coupling Coefficient Calculation for Ferrite-Based Matched Inductive Charging Systems," in *2019 IEEE Energy Conversion Congress and Exposition (ECCE)*, 29 Sept.-3 Oct. 2019 2019, pp. 1210-1214.

[16] J. Haruna, U. D. Kavimandan, O. Onar, V. P. Galigekere, and J. Pries, "Sensitivity Analysis of Compensation Topologies for Dynamic WPT System," in *2020 IEEE Transportation Electrification Conference & Expo (ITEC)*, 23-26 June 2020 2020, pp. 284-289.

[17] A. Rakhymbay, M. Bagheri, and M. Lu, "A simulation study on four different compensation topologies in EV wireless charging," in *2017 International Conference on Sustainable Energy Engineering and Application (ICSEEA)*, 23-24 Oct. 2017 2017, pp. 66-73.

[18] J. Zhang, X. Yuan, C. Wang, and Y. He, "Comparative Analysis of Two-Coil and Three-Coil Structures for Wireless Power Transfer," *IEEE Transactions on Power Electronics,* vol. 32, no. 1, pp. 341-352, 2017.

[19] W. X. Zhong, C. Zhang, X. Liu, and S. Y. R. Hui, "A Methodology for Making a Three-Coil Wireless Power Transfer System More Energy Efficient Than a Two-Coil Counterpart for Extended Transfer Distance," *IEEE Transactions on Power Electronics,* vol. 30, no. 2, pp. 933-942, 2015.

[20] Q. Wang and Y. Wang, "Power efficiency optimisation of a three-coil wireless power transfer using compensatory reactance," *IET Power Electronics,* vol. 11, no. 13, pp. 2102-2108, 2018.

[21] Z. Jian, Y. Xinmei, and W. Chuang, "A study of three-coil magnetically coupled resonators for wireless power transfer," in *2015 IEEE International Wireless Symposium (IWS 2015)*, 30 March-1 April 2015 2015, pp. 1-4.

[22] L. Yang, X. Li, S. Liu, Z. Xu, C. Cai, and P. Guo, "Analysis and Design of Three-Coil Structure WPT System With Constant Output Current and Voltage for Battery Charging Applications," *IEEE Access,* vol. 7, pp. 87334-87344, 2019.

[23] G. Zhu and D. Gao, "Effects of intermediate coil on power transfer capability and efficiency in three-coil wireless power transfer system," in *2017 IEEE Transportation Electrification Conference and Expo, Asia-Pacific (ITEC Asia-Pacific)*, 7-10 Aug. 2017 2017, pp. 1-6.

[24] M. Kiani, U. Jow, and M. Ghovanloo, "Design and Optimization of a 3-Coil Inductive Link for Efficient Wireless Power Transmission," *IEEE Transactions on Biomedical Circuits and Systems,* vol. 5, no. 6, pp. 579-591, 2011.

[25] Y. Ota, T. Takura, F. Sato, and H. Matsuki, "Wireless power transfer by low coupling electromagnetic induction — LC booster," in *2012 IEEE MTT-S International Microwave Workshop Series on Innovative Wireless Power Transmission: Technologies, Systems, and Applications*, 10-11 May 2012 2012, pp. 175-178.

[26] Q. Vo, Q. Duong, and M. Okada, "Cooperative Transmission in Three-Coil Inductive Power Transfer System with Load-Independent Output Voltages," in *2019 International Workshop on Antenna Technology (iWAT)*, 3-6 March 2019 2019, pp. 225-227.

[27] K. B. S. Kiran, M. Kumari, R. K. Behera, O. Ojo, and A. Iqbal, "Analysis and experimental verification of three-coil inductive resonant coupled wireless power transfer system," in *2017 National Power Electronics Conference (NPEC)*, 18-20 Dec. 2017 2017, pp. 84-89.

[28] Y. Li, Q. Xu, T. Lin, J. Hu, Z. He, and R. Mai, "Analysis and Design of Load-Independent Output Current or Output Voltage of a Three-Coil Wireless Power Transfer System," *IEEE Transactions on Transportation Electrification,* vol. 4, no. 2, pp. 364-375, 2018.

[29] Y. Zhang, T. Lu, and Z. Zhao, "Reducing the impact of source internal resistance by source coil in resonant wireless power transfer," in *2014 IEEE Energy Conversion Congress and Exposition (ECCE)*, 14-18 Sept. 2014 2014, pp. 845-850.

[30] W. Zhang and C. C. Mi, "Compensation Topologies of High-Power Wireless Power Transfer Systems," *IEEE Transactions on Vehicular Technology,* vol. 65, no. 6, pp. 4768-4778, 2016.

[31] Y. Zhang, Z. Yan, Z. Liang, S. Li, and C. C. Mi, "A High-Power Wireless Charging System Using LCL-N Topology to Achieve a Compact and Low-Cost Receiver," *IEEE Transactions on Power Electronics,* vol. 35, no. 1, pp. 131-137, 2020.

[32] P. Darvish, S. Mekhilef, and H. A. Illias, "A Novel S-S-LCLCC Compensation for Three-Coil WPT to Improve Misalignment and Energy Efficiency Stiffness of Wireless Charging System," *IEEE Transactions on Power Electronics,* pp. 1-1, 2020.

[33] Y. Liu, R. Mai, D. Liu, Y. Li, and Z. He, "Efficiency Optimization for Wireless Dynamic Charging System With Overlapped DD Coil Arrays," *IEEE Transactions on Power Electronics,* vol. 33, no. 4, pp. 2832-2846, 2018.